The Astrophysical Journal, 689:242–248, 2008 December 10

INTERSTELLAR WEATHER VANES: GLIMPSE MID-INFRARED STELLAR WIND BOW SHOCKS IN M17 AND RCW 49

Matthew S. Povich,[1] Robert A. Benjamin,[2] Barbara A. Whitney,[3] Brian L. Babler,[1]
Rémy Indebetouw,[4] Marilyn R. Meade,[1] and Ed Churchwell[1]
Received 2008 July 7; accepted 2008 August 11

ABSTRACT

We report the discovery of six infrared stellar wind bow shocks in the Galactic massive star formation regions M17 and RCW 49 from *Spitzer* GLIMPSE (Galactic Legacy Infrared Mid-Plane Survey Extraordinaire) images. The Infrared Array Camera (IRAC) on the *Spitzer Space Telescope* clearly resolves the arc-shaped emission produced by the bow shocks. We combine Two Micron All-Sky Survey (2MASS), *Spitzer*, *MSX*, and *IRAS* observations to obtain the spectral energy distributions (SEDs) of the bow shocks and their individual driving stars. We use the stellar SEDs to estimate the spectral types of the three newly identified O stars in RCW 49 and one previously undiscovered O star in M17. One of the bow shocks in RCW 49 reveals the presence of a large-scale flow of gas escaping the H II region at a few 10^2 km s^{-1}. Radiation transfer modeling of the steep rise in the SED of this bow shock toward longer mid-infrared wavelengths indicates that the emission is coming principally from dust heated by the star driving the shock. The other five bow shocks occur where the stellar winds of O stars sweep up dust in the expanding H II regions.

Subject headings: H II regions — infrared: ISM — shock waves — stars: mass loss

1. INTRODUCTION

The solar wind ends in a termination shock (e.g., Decker et al. 2005), where the pressure of the heliosphere balances the ram pressure of the surrounding interstellar medium (ISM). Massive stars with more energetic winds generate much stronger shocks. In cases where the relative motion between the star driving the wind and the ambient ISM is large, the shock will be bent back around the star. If the relative velocity is supersonic, the ambient ISM gas is swept into a second shock, forming an arc-shaped "bow shock" that is separated from the termination shock by a contact discontinuity. Stellar wind bow shocks have been reported for a variety of sources, including nearby runaway O stars (van Buren & McCray 1988; van Buren et al. 1995; Noriega-Crespo et al. 1997; Brown & Bomans 2005; Comerón & Pasquali 2007; France et al. 2007), high-mass X-ray binaries (Churchwell et al. 1992; Kaper et al. 1997; Huthoff & Kaper 2002), LL Ori–type stars (Bally et al. 2000), radio pulsars (Gaensler & Slane 2006), Galactic center O stars (Geballe et al. 2004, 2006), and mass-losing red giants (Martin et al. 2007). Recently, an infrared (IR) bow shock has been observed around the young A-type star δ Vel (Gáspár et al. 2008). Cometary H II regions also resemble bow shocks, due either to density gradients in the ambient gas or to the motion of the ionizing source with respect to the interstellar surroundings (van Buren et al. 1990; Arthur & Hoare 2006). Both the direction of a bow shock and its "standoff distance" from the star generating the wind are determined by the velocity of the star with respect to the surrounding medium. In the case of runaway O stars, this is dominated by the high space motion of the star.

We report the detection of three mid-IR bow shocks in each of two massive star formation regions: M17 and RCW 49. Two of the bow shocks in M17 are around known O stars. We will demonstrate that the other bow shocks are also around likely O stars. Since these stars are in or near expanding H II regions, we find that the direction of the bow shock is determined principally by the flow of the ISM rather than the space motion of the star.

2. OBSERVATIONS AND INTERPRETATION

The Galactic Legacy Infrared Mid-Plane Survey Extraordinaire (GLIMPSE; Benjamin et al. 2003) programs have mapped the inner Galactic midplane ($|l| \leq 65^\circ$) using the Infrared Array Camera (IRAC) instrument on the *Spitzer Space Telescope* (2″ resolution; Fazio et al. 2004). RCW 49, located at $(l, b) = (284.3, -0.3)$, was observed as part of the validation of the GLIMPSE observing strategy. The same area of the sky was imaged 10 times with 2 s exposures, and the combined data were mosaicked together to produce high-resolution images (0.6″ pixels) of this region in the four IRAC bands: 3.6, 4.5, 5.8, and 8.0 μm. An overview of these observations was given by Churchwell et al. (2004). M17, at $(l, b) = (15.0, -0.7)$, was included in the GLIMPSE survey area, with two visits on the sky combined to make mosaics with 0.6″ pixels.

2.1. *M17*

Povich et al. (2007) studied the diffuse emission morphology of M17 at multiple wavelengths from IR to radio, constraining the distance to 1.4–1.9 kpc. We will assume the widely adopted value of 1.6 kpc for the M17 distance, following Nielbock et al. (2001). The winds and radiation of the O stars in the NGC 6618 cluster have excavated a cavity in the center of the M17 H II region. The cavity is filled with hot, X-ray-emitting gas from shocked stellar winds (Townsley et al. 2003). Povich et al. (2007) noted the presence of three apparent stellar wind bow shocks along the northern wall of the cavity, along with a prominent "elephant trunk," or pillar, all oriented in the direction of the central ring of seven O stars in NGC 6618. These structures are highlighted in Figure 1, a GLIMPSE image of M17 with an enlargement of the

[1] Department of Astronomy, University of Wisconsin–Madison, 475 North Charter Street, Madison, WI 53706; povich@astro.wisc.edu.
[2] Department of Physics, University of Wisconsin–Whitewater, 800 West Main Street, Whitewater, WI 53190; benjamin@wisp.physics.wisc.edu.
[3] Space Science Institute, 3100 Marine Street, Suite A353, Boulder, CO 80303-1058.
[4] Department of Astronomy, University of Virginia, Charlottesville, VA 22903-0818.

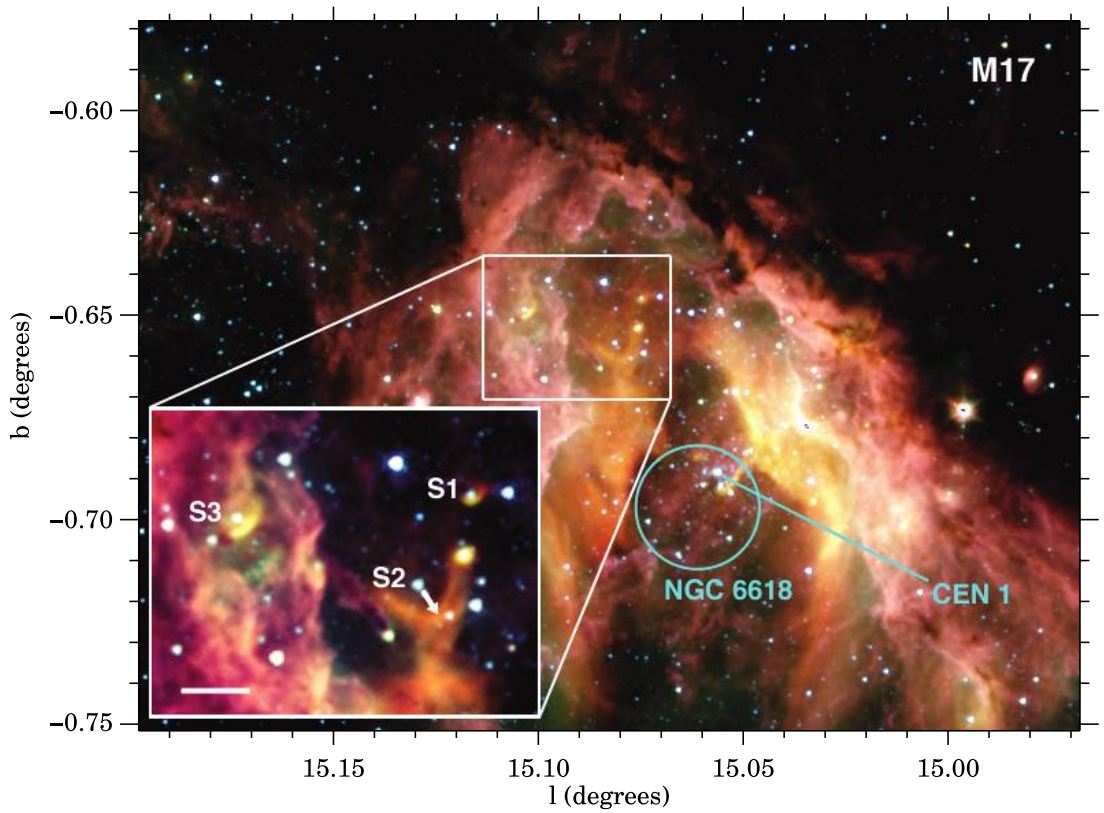

FIG. 1.—GLIMPSE full-color image of M17 (*blue*: 3.6 μm; *green*: 4.5 μm; *orange*: 5.8 μm; *red*: 8.0 μm). The region containing the bow shocks M17-S1, M17-S2, and M17-S3 is enlarged (scale bar shows $30'' = 0.23$ pc at 1.6 kpc). The central ring of O stars in the NGC 6618 cluster is circled. The bow shocks, along with the prominent pillar structure near M17-S2, all appear to be oriented in the general direction of CEN 1, the O4-O4 binary system in the center of the ionizing cluster.

region containing the bow shocks. The bow shocks stand out as yellow-orange features in the image because they are faint at 3.6 μm (*blue*) compared to the other three IRAC bands.

We designate these stellar wind bow shocks in Figure 1 with the name of the region followed by an identification number, in order of increasing Galactic longitude (for example, M17-S1). IR fluxes for all of the bow shock driving stars are given in Table 1, and background-subtracted IR fluxes from aperture photometry of the bow shocks are listed in Table 2. Spectral types of two of the driving stars have been determined photometrically (Bumgardner 1992) and spectroscopically (Hanson et al. 1997). M17-S1 is associated with CEN 16, an O9-B2 star. The larger bow shock, M17-S2, is driven by CEN 18, an earlier type star (O7-O8). Both bow shocks were detected at 10.5 and 20 μm by Nielbock et al. (2001). These observations did not resolve the arc shapes of the bow shocks, and Nielbock et al. (2001) attributed the excess IR emission to circumstellar disks and classified CEN 16 and IRS 9 (the star visible just to the right of the arrowhead in Fig. 1) as massive protostars.

M17-S3 lies outside of the field analyzed by Hanson et al. (1997), and the driving star does not appear in any catalog of the region. It is not found in any GLIMPSE source list, because the bright, spatially variable diffuse background prevented the automatic extraction of the point source. We measured the flux of this source manually using a 5″ aperture. Using the spectral energy distribution (SED) fitting tool of Robitaille et al. (2007) we fit the

TABLE 1
2MASS AND IRAC IR FLUXES FOR BOW SHOCK DRIVING STARS (mJy)

ID No.	l	b	$F[J]$	$F[H]$	$F[K]$	$F[3.6]$	$F[4.5]$[a]	$F[5.8]$[a]
M17-S1	15.07486	−0.64607	196	214	186	96	67	...
M17-S2	15.08126	−0.65699	427	534	495	257	181	120
M17-S3[b]	15.10325	−0.64867	103	200	238	151	≤154	≤155
RCW 49-S1.....	284.07646	−0.43228	24	40	46	28	21	15
RCW 49-S2.....	284.30107	−0.37121	10	18	20	13	≤11	≤27
RCW 49-S3.....	284.33999	−0.28269	83	97	90	47	32	27

NOTE.—None of these stars were detected in the IRAC [8.0] band.

[a] In cases where bow shock emission appears to cause a mid-IR excess over the stellar spectrum, the [4.5] and [5.8] fluxes are reported as upper limits. Due to suspected contamination from the bow shock or other diffuse emission, these fluxes are treated as upper limits to the stellar flux.

[b] Because the star driving SWB M17-3 is surrounded by bright, complex diffuse background emission, it was not extracted as part of the GLIMPSE point-source catalog. The fluxes reported here were measured using aperture photometry.

TABLE 2
IR Fluxes for Bow Shocks (mJy)

ID No.	l_{apex}	b_{apex}	IRAC Fluxes[a]			
			F[3.6][b]	F[4.5]	F[5.8]	F[8.0]
M17-S1	15.0744	−0.6465	≤34	71 ± 9	252 ± 42	1110 ± 290
M17-S2	15.0791	−0.6613	43 ± 17	245 ± 48	1240 ± 159	8700 ± 1500
M17-S3	15.1026	−0.6503	69 ± 16	240 ± 19	620 ± 100	1800 ± 320
RCW 49-S1.....	284.0775	−0.4305	5.7 ± 0.9	12 ± 1	33 ± 1	322 ± 5
RCW 49-S2.....	284.3018	−0.3712	≤2	9.6 ± 0.5	32 ± 3	172 ± 7
RCW 49-S3.....	284.3388	−0.2829	≤21	50 ± 7	160 ± 20	825 ± 120
MSX Fluxes[c]						
			F[8.3]	F[12.1]	F[14.6]	F[21.3]
RCW 49-S1.....	MSXC6 Name	G284.0776−00.4340	627	2729	5674	1.56×10^4
IRAS Fluxes[c]						
			F[12]	F[25]	F[60]	F[100]
RCW 49-S1.....	*IRAS* Name	IRAS 10205−5729	3810	4.21×10^4	$\leq 2.26 \times 10^5$	2.75×10^5

[a] The IRAC fluxes are background-subtracted. Fluxes were measured using irregular apertures drawn to enclose all of the visible bow shock structure. Separate apertures were used to estimate the background flux. For each bow shock, the same set of apertures was used for all IRAC wavelengths.
[b] In cases where stellar emission appears to be confused with bow shock emission, the [3.6] bow shock fluxes reported are upper limits only.
[c] RCW 49-S1 is a point source in both the *MSX* and *IRAS* catalogs. All of the other bow shocks are confused with bright diffuse background IR emission features at the resolutions of *MSX* and *IRAS*.

IR fluxes of this star (Table 1) with Kurucz (1993) stellar atmosphere models. Following the method described by Watson et al. (2008) we scale the models to the 1.6 kpc distance of M17 and estimate a spectral type of O7 V for the star. Carrying out the same analysis on seven other O stars in M17 with independently known spectral types (Povich et al. 2008), we estimate that our spectral typing is accurate to within two subclasses.

2.2. *RCW 49*

RCW 49 presents a more complicated morphology than M17. Churchwell et al. (2004) discussed the structure and spectrum of the diffuse emission. Like M17, RCW 49 is filled with X-ray gas (Townsley et al. 2005). The interstellar structures are dominated by two large cavities. The first, blown out to the west, contains the massive young cluster Westerlund 2, and the second is an enclosed bubble around the Wolf-Rayet star WR 20b (Fig. 2). The distance to RCW 49 remains disputed, with recent estimates placing the region as close as 2.8 kpc (Ascenso et al. 2007) or as far as 8.0 kpc (Rauw et al. 2007), with a kinematic distance estimate of 6 ± 1 kpc (Dame 2007). We consider distances of both 4.2 kpc (Churchwell et al. 2004) and 6 kpc in our analysis.

We have found three bow shocks associated with RCW 49, shown in three separate insets in Figure 2. RCW 49-S1 is unique among our sample, because it lies relatively far from the H II region, but we believe it is associated with RCW 49 for the following reasons: (1) the RCW 49 distance is consistent with the luminosity of the driving star being an O star (see below); and (2) the bow shock points (approximately) toward the central cluster, Westerlund 2. Because it is far from any other bright IR source, RCW 49-S1 appears as a point source in both the *Midcourse Space Experiment* (*MSX*; Price et al. 2001) and *Infrared Astronomical Satellite* (*IRAS*; Beichman et al. 1988) Point Source Catalogs, and these fluxes are also given in Table 2.

RCW 49-S2 is oriented away from Westerlund 2 and appears to be influenced primarily by the nearby WR 20b. RCW 49-S3 is oriented in the general direction of Westerlund 2. None of the RCW 49 bow shocks point directly back toward the central cluster, while all three M17 bow shocks do. Perhaps the expanding bubbles driven by Westerlund 2 and the Wolf-Rayet stars are interacting turbulently, producing nonradial components to the flows. It is also possible that the bow shock driving stars have large orbital motions relative to the dynamic interstellar medium.

The three bow shock driving stars in RCW 49 are of previously undetermined spectral type, so we again estimate the spectral type by fitting model SEDs to the broadband fluxes of Table 1, scaled to both the 4.2 and 6 kpc distances. The results are given in Table 3. All three stars are plausibly O stars. Assuming 4.2 kpc, the driving star of RCW 49-S1 is fit as O6 V, RCW 49-S2 as O 9 V, and RCW 49-S3 as O5 V (or O9 III). If we increase the distance to 6 kpc, the fits become O 5 III, O6 V, and O5 V (or O6.5 III), respectively (see Watson et al. [2008] for an explanation of the degeneracy between luminosity classes). The spectral types at 6 kpc seem improbably luminous. Highly luminous and windy stars dominate the dynamics of their local ISM. We do not observe IR bow shocks around any of the earliest type stars in either RCW 49 or M17, because they have blown large, evacuated cavities in the centers of the H II regions. Little or no ambient material remains close to the stars to produce a bow shock.

Apart from the Wolf-Rayet systems, one of the earliest stars in RCW 49 is G284.2642−00.3156. Using optical spectroscopy, Uzpen et al. (2005) classified this star as O4 V(f) and derived a spectrophotometric distance of 3.2 ± 0.5 kpc. Using IR SED fitting, we confirm that the luminosity of this star is consistent with an O4 V star at 3.2 kpc. Yet this distance falls on the low end of the range of published distance estimates for RCW 49, and we do not adopt it here. Like CEN 1 in M17, G284.2642−00.3156 may be an unresolved, equal-mass O4-O4 binary. Doubling the luminosity moves the spectrophotometric distance from 3.2 to 4.5 kpc, in agreement with a distance of 4.2 kpc but inconsistent with 6 kpc.

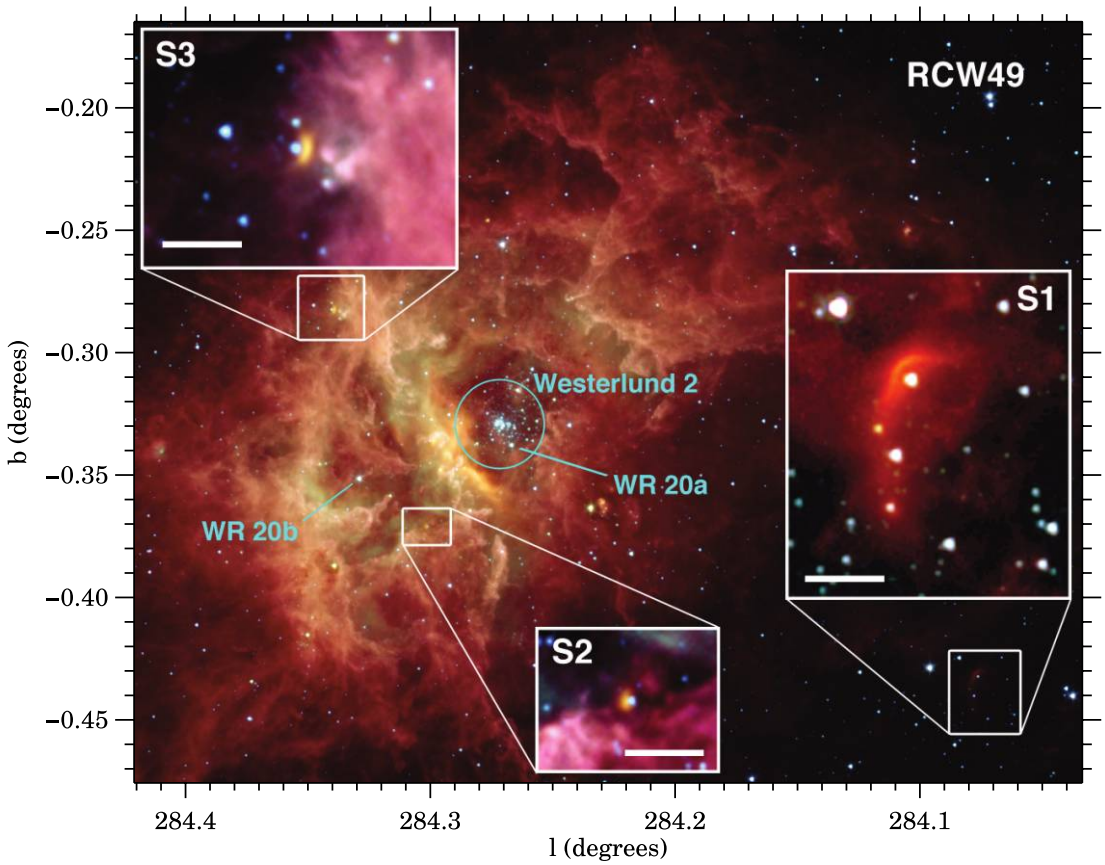

FIG. 2.—GLIMPSE full-color image of RCW 49 (*blue*: [3.6]; *green*: [4.5]; *orange*: [5.8]; *red*: [8.0]). The bow shocks RCW 49-S1, RCW 49-S2, and RCW 49-S3 are enlarged in three separate insets (scale bars are $30'' \approx 0.6$ pc at 4.2 kpc). Three energy sources that could drive large-scale interstellar flows are also indicated: the Westerlund 2 cluster (*circled*), and the Wolf-Rayet stars WR 20a and WR 20b.

TABLE 3

BOW SHOCK STANDOFF DISTANCES AND ESTIMATED STELLAR WIND PROPERTIES

ID No.	Spectral Type[a]	$\dot{M}_{w,-6} v_{w,8}$[b]	$d_w \cos i$ (pc)	$d_{cl} \cos i$ (pc)	$v_0 n^{1/2}{}_{0,3} (\cos i)^{-1}$ (km s^{-1})
M17 Distance = 1.6 kpc					
M17-S1	O9-B2 V	$\leq$0.2	0.03	1.4	$\leq$22
M17-S2	O7-O8 V	0.5–2.5	0.11	0.9	10–22
M17-S3	O7 V	0.5–2.5	0.05	1.7	21–47
RCW 49 Distance = 4.2 kpc					
RCW 49-S1.....	O6 V	~1.3	0.16	16.2	11
RCW 49-S2.....	O9 V	~0.2	0.04	2.46	17
RCW 49-S3.....	O5 V or O9 III	2.5–3.2	0.096	6.13	25–28
RCW 49 Distance = 6.1 kpc					
RCW 49-S1.....	O5 III	~16	0.23	23.2	26
RCW 49-S2.....	O6 V	~1.3	0.06	3.52	28
RCW 49-S3.....	O3 V or O6.5 III	>3.2	0.14	8.8	>19

[a] Spectral types for the stars driving M17-S1 and M17-S2 are taken from Chini et al. (1980 [CEN]) and Hanson et al. (1997). All others were estimated by fitting Kurucz (1993) stellar atmosphere models to the broadband IR fluxes (Table 1) and scaling to the distance of M17 or RCW 49. Spectral types given for RCW 49 are highly uncertain due to the disputed distance to that region.

[b] Estimates of stellar mass-loss rates $\dot{M}_{w,-6} = \dot{M}_w/(10^{-6}\ M_\odot\ \mathrm{yr}^{-1})$ and wind velocities $v_{w,8} = v_w/(10^8\ \mathrm{cm\ s}^{-1})$ are based on Vink et al. (2001) and Fullerton et al. (2006).

3. BOW SHOCK PROPERTIES

The standoff distance d_w of a bow shock from its driving star is the point where the momentum flux of the stellar wind balances the momentum flux of the ambient medium: $n_w v_w^2 = n_0 v_0^2$. Following van Buren & McCray (1988) we normalize the stellar wind mass-loss rate, $\dot{M}_{w,-6} = 10^{-6}\ M_\odot\ \mathrm{yr}^{-1}$, stellar wind velocity $v_{w,8} = 10^8\ \mathrm{cm\ s}^{-1}$, ambient hydrogen particle density of $n_{0,3} = 10^3\ \mathrm{cm}^{-3}$, and use a mean ISM gas mass per hydrogen atom, $\mu = 2.36 \times 10^{-24}$ g. Assuming a spherically symmetric stellar wind with a mass-loss rate given by $\dot{M} = 4\pi d_w^2 \mu n_w v_w$, the velocity of the star with respect to the ambient ISM can be written as

$$v_0 = 1.5 \left(\frac{d_w}{\mathrm{pc}}\right)^{-1} (\dot{M}_{w,-6} v_{w,8})^{1/2} n_{0,3}^{-1/2}\ [\mathrm{km\ s}^{-1}], \qquad (1)$$

where v_w is the terminal velocity of the stellar wind. Values of $v_0 n_{0,3}^{1/2}$ and d_w for each bow shock are presented in Table 3. The standoff distance can be measured only as $d_w \cos i$ on the sky, where i is the inclination (or viewing angle) made by the line connecting the star with the apex of the bow shock against the plane of the sky ($i = 0$ if the line joining the star to the bow shock apex lies in the plane of the sky). Because a bow shock oriented at high i will not produce an arc morphology, it is likely that $i \lesssim 45^\circ$, and hence $\cos i$, will not differ greatly from unity in our measurements.[5] The distance from each bow shock to the likely source of the large-scale ISM flow, measured on the sky as $d_{cl} \cos i$, are also presented for reference in Table 3.

The mass-loss rates and stellar wind velocities in equation (1) suffer from high dispersion as a function of spectral type (Fullerton et al. 2006), a factor of 2 or even greater, and this is compounded by a comparable level of uncertainty in the spectral types. The uncertainty on our measurements of d_w ranges from ∼20% for the largest bow shocks (M17-S2 and RCW 49-S1) to ∼40% for the smaller bow shocks that are barely resolved by IRAC. We estimate that $v_0 n_0^{1/2}$ is uncertain by a factor of 2 in M17 and up to a factor of 3 in RCW 49, where the spectral types of the driving stars are less constrained. These uncertainties, reflected in the range of values for $v_0 n_0^{1/2}$ in Table 3, are dominated by the uncertainty in the stellar wind properties.

We have neglected the effects of turbulent pressure in our calculation of the momentum flux balance of the bow shocks. This is a potentially significant contributor to the total ISM pressure held off by the bow shocks. The effect of turbulent pressure would be to systematically decrease the standoff distance d_w, causing us to overestimate v_0.

In reality, for the fast winds of early-type stars, the observed bow shock is displaced from the standoff distance by a significant amount. This happens because the cooling timescale of the shocked stellar wind is very long. The result is a thick layer of hot gas intervening between the wind terminal shock at the standoff distance and the thin, dense layer of interstellar gas and dust forming the observed bow shock. The numerical simulations of Comerón & Kaper (1998) predict that the bow shock should be located at twice the standoff distance from the driving star. In this case, our derived values of $v_0 n_0^{1/2}$ in Table 3 would be underestimated by the same factor of 2. This systematic correction is comparable to the intrinsic uncertainties in our estimates of $v_0 n_0^{1/2}$, and it partially compensates for the effects of neglecting turbulent pressure in the ambient ISM. Therefore, the assumption that the observed distance of the bow shocks from the driving stars corresponds to the standoff distance d_w should not have a large impact on our results, and we find that the cautious application of equation (1) yields reasonable results.

Orbital velocities of O stars in massive clusters are typically <10 km s^{-1}. The expansion speed of ionized gas in H II regions is generally comparable to the sound speed of ∼10 km s^{-1}, and this appears to be true in M17 (Pellegrini et al. 2007). Most of the bow shocks (the exception being RCW 49-S1) are apparently located within the ionized gas of the radio H II regions. The likely explanation for the bow shock emission in the IR is that dust in the H II regions (Povich et al. 2007) is swept up by the bow shocks. The observed average electron density in the northern bar of the M17 H II region is $\sim 10^3\ \mathrm{cm}^{-3}$ (Felli et al. 1984), so the values of $v_0 n_{0,3}^{1/2}$ listed in Table 3 are likely to be close to the actual relative velocities of the stars and the ISM for most of the bow shocks.

The values of $v_0 n_{0,3}^{1/2}$ calculated for M17-S1 and M17-S2 are in good agreement. M17-S3, however, presents a different picture. M17-S3 appears to be associated with a "teardrop" structure (Fig. 1) in the photodissociation region (PDR), near the ionization front. The ambient density surrounding this star could be significantly higher than the density within the H II region. If v_0 for this bow shock is comparable to that of the other two bow shocks in M17, then $n_{0,3} \sim 2.25\ \mathrm{cm}^{-3}$ in this location. This value agrees with the measurements of electron density in the dense clumps of ionized gas in M17 (Felli et al. 1984). The unusual morphology of the diffuse IR emission associated with M17-S3 suggests that the star may have recently emerged from an evaporating globule on the edge of the PDR: a larger, more evolved analog of the nearby pillar structure seen in Figure 1.

In RCW 49, all three bow shocks are found in very different locations, but we note that two of the bow shocks appear to be similar in size, color, and ambient environment (Fig. 2). The largest bow shock, RCW 49-S1, is different, since it is located relatively far (16.2 pc at 4.2 kpc) from Westerlund 2, outside the H II region. The presence of RCW 49-S1, along with its orientation, indicates that RCW 49 vents a large-scale flow of gas through the cavity opening to the west. This flow likely originates in the combined winds of the Westerlund 2 cluster and thus should be much more diffuse than the H II region gas (Townsley et al. 2003, 2005). Assuming a density of 1 cm^{-3} in the flow from Westerlund 2, the standoff distance of RCW 49-S1 at 4.2 kpc gives a flow velocity of ∼350 km s^{-1}. Such a high value of v_0 is reasonable, given that the gas must move supersonically relative to the star to produce a shock, and the sound speed in the hot, rarefied gas of the flow streaming away from the H II region is ∼100 km s^{-1}.

Because RCW 49-S1 was detected by *MSX* and *IRAS* in addition to GLIMPSE, we can construct the SED of the bow shock from 4.5 to 100 μm (Table 2). We computed SED models of RCW 49-S1 using a three-dimensional radiative equilibrium code (Whitney et al. 2003) modified to include very small grain (VSG) and polycyclic aromatic hydrocarbon (PAH) emission (Wood et al. 2008). We used the canonical mass fraction for VSG/PAH grains of 5% (Draine & Li 2007). We modeled the bow shock geometry as a paraboloid with the apex offset by $d_w = 0.16$ pc from the O6 V star (assuming $i = 0$ and the 4.2 kpc distance). For models that reproduced the observed images, the SED shape was insensitive both to the thickness of the shock and to the radial density profile of the dust (with the total mass scaled to match the observed SED). The black line in Figure 3 shows the SED for a model with a density varying as r^{-2} from the 0.16 pc standoff distance out to a radius of 1.5 pc. The observed SED shortward of 30 μm is well matched by the model. For radial density exponents from −2 to zero, the mass of this material ranges from ∼0.5 to 2 $M_\odot$, respectively, assuming a dust–to–gas mass ratio

[5] The average value of cos$i$ for $0 \le i \le 45^\circ$ is 0.9.

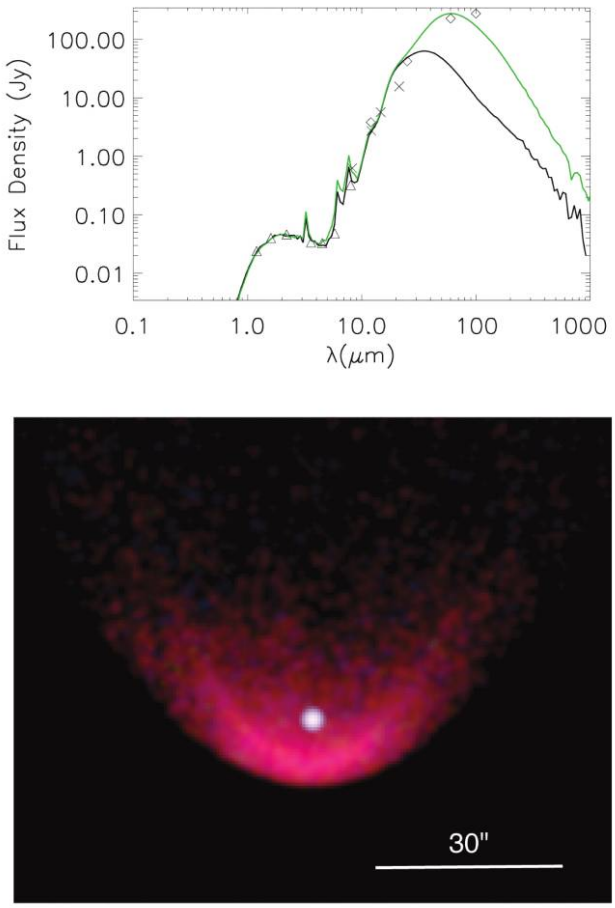

FIG. 3.—Radiation transfer model of RCW 49-S1. *Top*: Model SEDs plotted with the fluxes of the bow shock and driving star from Tables 1 and 2 (*triangles*: 2MASS and GLIMPSE; *crosses*: *MSX*; *diamonds*: *IRAS*). The green curve includes low-density material in a shell 2–3 pc from the star in order to match the *IRAS* 60 and 100 μm fluxes. *Bottom*: Image of the model bow shock at GLIMPSE wavelengths (compare to Fig. 2).

of 0.01. The optical depth in all models is low, with $A_V < 0.02$ within 1 pc. To match the *IRAS* data at 60 and 100 μm requires low-density material farther from the star. The green line in Figure 3 is a model including a shell 2–3 pc from the star. This material added mid-IR PAH emission, so we lowered the VSG/PAH mass fraction to 3% to continue to match the mid-IR SED, and the image still matches the data well. The A_V through the bow shock in this model is 0.25, most of it due to the outer shell. Along the line of sight to the star, $A_V = 10$, so the bow shock and shell contribute a negligible fraction of the interstellar extinction. These models show that dust distributed in a bow shock geometry matches both the images and the SED reasonably well. The IR emission from the bow shock can be explained by reprocessed stellar radiation without any additional dust heating by the shock.

The structure of RCW 49-S1 is probably significantly different from that of the other five bow shocks in our sample, because it is located in a distinct interstellar environment. Because of the high temperature and low density in the flow outside the H II region, the shocked interstellar gas cannot cool quickly enough to form a dense layer behind the bow shock, as likely happens in the other five cases. The shock is approximately adiabatic, remaining very hot and only moderately compressed (by a factor of $\sim$4) as it flows past the star, forming a relatively thick layer. Hence, while RCW 49-S1 is the only bow shock in our sample observed at enough different mid-IR wavelengths to allow us to create a meaningful model of the emission, it may not be appropriate to draw strong conclusions about the remaining bow shocks based on this model.

4. SUMMARY

We have observed six prominent IR bow shocks in M17 and RCW 49. These objects appear to be produced by the winds of individual O stars colliding with large-scale interstellar gas flows in the H II regions. One bow shock, M17-S3, may be the leading edge of an evaporating globule containing a newly formed and previously undiscovered O star in the well-studied M17 region. All three bow shocks associated with RCW 49 lead us to identify new candidate O stars. Our stellar classifications also suggest that the true distance to RCW 49 is less than the kinematic distance of 6 kpc.

The bow shocks are bright at IR wavelengths due to emission from dust swept up from the ambient ISM and heated by radiation from the bow shock driving stars. As Gáspár et al. (2008) note, IR excess emission from a bow shock could be attributed to the presence of a circumstellar disk, particularly when the bow shock morphology is not spatially well resolved. This can be a pitfall for observational studies of accreting massive protostars.

The collective winds of the most luminous stars in young, massive clusters produce overlapping large-scale flows that hollow out thermally hot cavities in the parent molecular cloud (Townsley et al. 2003). The largest bow shock presented here, RCW 49-S1, is evidence that the combined winds of the ionizing stars in Westerlund 2 have escaped the H II region, creating a flow of hot gas moving at a few 10^2 km s^{-1} that extends at least 16 pc away from RCW 49.

The driving stars of the other five bow shocks are surrounded by ionized gas and dust of their natal H II regions, where the density of the ambient medium ($n_0 \sim 10^3$ cm^{-3}) is sufficiently high to produce the observed bow shocks with a relative velocity of only 10–20 km s^{-1}. The winds of the bow shock driving stars do not directly encounter the >2000 km s^{-1} winds from the most massive stars in the cluster. Instead, the bow shocks are shaped by the expansion of the ionized gas in the H II regions relative to the orbital motions of the stars.

Eventually, supernova explosions will produce high-velocity shock waves that heat and disperse the original gas cloud. In star-forming regions like M17 and RCW 49 that have not yet been disrupted by supernovae, IR bow shocks serve as interstellar "weather vanes," indicating the speed and direction of large-scale gas flows at points within and around giant H II regions.

We thank the anonymous referee for incisive and very useful suggestions that helped us improve this work. We are grateful to Joseph Cassinelli, Eric Pellegrini, John Raymond, Ellen Zweibel, Heidi Gneiser, and Don Cox for useful conversations while preparing this paper. M. S. P. thanks the members of the "dissertator club," Kathryn Devine, K. Tabetha Hole, and Nicholas Murphy, for their helpful comments. This work was supported by NSF grant AST 03-0368 (E. B. C.) and NASA/JPL contracts 1282620 and 1298148. Additional support was provided by the NASA Theory Program (NNG 05GH35G; B. A. W.). R. I. acknowledges support from a *Spitzer* Fellowship at the time that these data were analyzed, and from JPL RSA1275467.

REFERENCES

Arthur, S. J., & Hoare, M. G. 2006, ApJS, 165, 283
Ascenso, J., Alves, J., Beletsky, Y., & Lago, M. T. V. T. 2007, A&A, 466, 137
Bally, J., O'Dell, C. R., & McCaughrean, M. J. 2000, AJ, 119, 2919
Beichman, C. A., Neugebauer, G., Habing, H. J., Clegg, P. E., & Chester, T. J., eds. 1988, *IRAS* Catalogs and Atlases, Vol. 1: Explanatory Supplement (NASA RP-1190; Washington: NASA)
Benjamin, R. A., et al. 2003, PASP, 115, 953
Brown, D., & Bomans, D. J. 2005, A&A, 439, 183
Bumgardner, T. E. 1992, M. S. thesis, Ohio State Univ. (Columbus)
Chini, R., Elsässer, H., & Neckel, T. 1980, A&A, 91, 186 (CEN)
Churchwell, E., Bieging, J. H., van der Hucht, K. A., Williams, P. M., Spoelstra, T. A. T., & Abbott, D. C. 1992, ApJ, 393, 329
Churchwell, E., et al. 2004, ApJS, 154, 322
Comerón, F., & Kaper, L. 1998, A&A, 338, 273
Comerón, F., & Pasquali, A. 2007, A&A, 467, L23
Dame, T. M. 2007, ApJ, 665, L163
Decker, R. B., et al. 2005, Science, 309, 2020
Draine, B. T., & Li, A. 2007, ApJ, 657, 810
Fazio, G. G., et al. 2004, ApJS, 154, 10
Felli, M., Churchwell, E., & Massi, M. 1984, A&A, 136, 53
France, K., McCandliss, S. R., & Lupu, R. E. 2007, ApJ, 655, 920
Fullerton, A. W., Massa, D. L., & Prinja, R. K. 2006, ApJ, 637, 1025
Gaensler, B. M., & Slane, P. O. 2006, ARA&A, 44, 17
Gáspár, A., Su, K. Y. L., Rieke, G. H., Balog, Z., Kamp, I., Martínex-Galarza, J. R., & Stapelfeldt, K. 2008, ApJ, 672, 974
Geballe, T. R., Najarro, F., Rigaut, F., & Roy, J.-R. 2006, ApJ, 652, 370
Geballe, T. R., Rigaut, F., Roy, J.-R., & Draine, B. T. 2004, ApJ, 602, 770
Hanson, M. M., Howarth, I. D., & Conti, P. S. 1997, ApJ, 489, 698
Huthoff, F., & Kaper, L. 2002, A&A, 383, 999
Kaper, L., van Loon, J. T., Augusteijn, T., Goudfrooij, P., Patat, F., Waters, L. B. F. M., & Zijlstra, A. A. 1997, ApJ, 475, L37
Kurucz, R. 1993, CD-ROM 13, ATLAS9 Stellar Atmosphere Programs and 2 km/s Grid (Cambridge: SAO)
Martin, D. C., et al. 2007, Nature, 448, 780
Nielbock, M., Chini, R., Jütte, M., & Manthey, E. 2001, A&A, 377, 273
Noriega-Crespo, A., van Buren, D., & Dgani, R. 1997, AJ, 113, 780
Pellegrini, E. W., et al. 2007, ApJ, 658, 1119
Povich, M. S., et al. 2007, ApJ, 660, 346
———. 2008, ApJ, submitted
Price, S. D., Egan, M. P., Carey, S. J., Mizuno, D. R., & Kuchar, T. A. 2001, AJ, 121, 2819
Rauw, G., Manfroid, J., Gosset, E., Nazé, Y., Sana, H., De Becker, M., Foellmi, C., & Moffat, A. F. J. 2007, A&A, 463, 981
Robitaille, T. P., Whitney, B. A., Indebetouw, R., & Wood, K. 2007, ApJS, 169, 328
Townsley, L., Feigelson, E., Montmerle, T., Broos, P., Chu, Y.-H., Garmire, G., & Getman, K. 2005, in X-Ray and Radio Connections, ed. L. O. Sjouwerman & K. K. Dyer (Santa Fe: NRAO), http://www.aoc.nrao.edu/events/xraydio
Townsley, L. K., Feigelson, E. D., Montmerle, T., Broos, P. S., Chu, Y.-H., & Garmire, G. P. 2003, ApJ, 593, 874
Uzpen, B., et al. 2005, ApJ, 629, 512
van Buren, D., Mac Low, M. M., Wood, D. O. S., & Churchwell, E. 1990, ApJ, 353, 570
van Buren, D., & McCray, R. 1988, ApJ, 329, L93
van Buren, D., Noriega-Crespo, A., & Dgani, R. 1995, AJ, 110, 2914
Vink, J. S., de Koter, A., & Lamers, H. J. G. L. M. 2001, A&A, 369, 574
Watson, C., et al. 2008, ApJ, 681, 1341
Whitney, B. A., Wood, K., Bjorkman, J. E., & Wolff, M. J. 2003, ApJ, 591, 1049
Wood, K., Whitney, B. A., Robitaille, T. P., & Draine, B. T. 2008, ApJ, 688, 1118

Note added in proof.—It has recently come to our attention that the RCW 49-S1 bow shock is located on the rim of a large radio blister associated with RCW 49 (J. B. Z. Whiteoak & K. I. Uchida, A&A, 317, 563 [1997]). This provides additional evidence for the existence of a large-scale gas flow escaping the RCW 49 H II region that is interacting with the stellar wind of the O star and producing the bow shock.